

Article

Feasibility of Microbially Induced Carbonate Precipitation to Enhance the Internal Stability of Loess under Zn-Contaminated Seepage Conditions

Pengli He ^{1,*}, Jinjun Guo ¹ and Shixu Zhang ²

¹ School of Civil Engineering, Luoyang Institute of Science and Technology, Luoyang 471023, China; guojinjun@lit.edu.cn

² School of Civil Engineering, Xi'an University of Architecture and Technology, Xi'an 710055, China; zhangsx@xauat.edu.cn

* Correspondence: hhzhly@lit.edu.cn

Abstract: Loess is widely distributed in Northwestern China and serves as the preferred engineering construction material for anti-fouling barriers. Heavy metal contamination in soil presents significant challenges to the engineering safety of vulnerable loess structures. Hence, there is an urgent need to investigate the impact of heavy metal ions on their percolation performance. In order to investigate the effectiveness of microbially induced carbonate precipitation (MICP) using *Sporosarcina pasturii* (CGMCC1.3687) bacteria in reducing internal seepage erosion, a saturated permeability test was conducted on reshaped loess under constant water head saturation conditions. The response of loess to deionized water (DW) and ZnCl₂ solution seepages was analyzed by monitoring changes in cation concentration over time, measuring Zeta potential, and using scanning electron microscopy (SEM). The results indicate that the hydrolysis of Zn²⁺ creates an acidic environment, leading to the dissolution of carbonate minerals in the loess, which enhances its permeability. The adsorption of Zn²⁺ ions and the resulting diffusion double-layer (DDL) effect reduce the thickness of the diffusion layer and increase the number of free water channels. Additionally, the permeability of loess exposed to ZnCl₂ solution seepage significantly increased by 554.5% compared to loess exposed to deionized water (DW) seepage. Following the seepage of ZnCl₂ solutions, changes in micropore area ratio were observed, decreasing by 48.80%, while mesopore areas increased by 23.9%. MICP treatment helps reduce erosion and volume shrinkage in contaminated loess. Carbonate precipitation enhances the erosion resistance of contaminated loess by absorbing or coating fine particles and creating bridging connections with coarse particles. These research results offer new perspectives on enhancing the seepage properties of saturated loess in the presence of heavy metal erosion and the geochemical mechanisms involved.

Keywords: seepage behavior; Q₃ loess; Zn contamination; microstructure; microbially induced carbonate precipitation (MICP)



Citation: He, P.; Guo, J.; Zhang, S. Feasibility of Microbially Induced Carbonate Precipitation to Enhance the Internal Stability of Loess under Zn-Contaminated Seepage Conditions. *Buildings* **2024**, *14*, 1230. <https://doi.org/10.3390/buildings14051230>

Academic Editor: Bjorn Birgisson

Received: 23 March 2024

Revised: 15 April 2024

Accepted: 23 April 2024

Published: 26 April 2024



Copyright: © 2024 by the authors. Licensee MDPI, Basel, Switzerland. This article is an open access article distributed under the terms and conditions of the Creative Commons Attribution (CC BY) license (<https://creativecommons.org/licenses/by/4.0/>).

1. Introduction

Loess, which covers approximately 9.3% of the Earth's land surface, is commonly found in arid and semi-arid regions [1–3]. It is utilized in various engineering projects for foundations, building materials, and constructing underground anti-fouling barriers to treat heavy metal-contaminated soil. However, interactions between contaminated liquids and loess can modify pore structure, deteriorate soil engineering properties, and negatively impact the performance of anti-fouling barriers [4]. Understanding these mechanisms and implementing strategies to improve heavy metal-contaminated soil are crucial for ensuring the safety and longevity of geotechnical engineering projects [5].

In recent years, environmental geotechnical engineering has recently seen a growing emphasis on the effects of heavy metal contamination on soil properties. Wu et al. [6]

provided a comprehensive overview of the changes in material composition and physical and chemical properties of heavy metal-contaminated soil. Gajo and Maines [7] noted a decrease in the Atterberg limit when heavy metal ions are introduced to soil. Various studies have explored the impact of heavy metal ions on soil permeability, shear strength, and compressive strength. Despite extensive research by Xu et al. [8], Zeng et al. [9], and Liu et al. [10] on different properties of contaminated soil, a gap still exists in understanding the seepage mechanism of contaminated soil. The permeability of loess is crucial in determining its resistance to seepage and contamination, especially in NW China [10]. Contaminants primarily enter the soil through seepage, where they migrate and transform. Heavy metal contamination during seepage changes the chemical properties of pore water, leading to complex soil–water interactions that degrade soil engineering performance. The permeability coefficient of reshaped loess is a key indicator for evaluating the flow of contaminated liquids in engineering projects [8,11]. Therefore, it is essential to investigate the seepage characteristics and underlying mechanisms of heavy metal-contaminated loess in environmental geotechnical engineering.

Various methods have been proposed and implemented to address internal erosion and seepage, such as chemical stabilization and seepage control techniques. While these methods can effectively reduce internal erosion under specific conditions, challenges like inadequate permeability control and the need for significant excavation and installation work have been identified. For instance, Feng and Montoya (2016) highlighted that the installation of protective drainage channels and slurry trenches in existing structures for erosion and water seepage prevention necessitates extensive construction work. Microbially induced carbonate precipitation (MICP) is a biomineralization process induced by bacteria that has been extensively researched in civil, environmental, and infrastructure engineering applications [12–16]. The hydrolysis of urea by native or introduced ureagenic bacteria such as *Pasteurella* and *Bacillus megaterium* is a common pathway for biologically mediated carbonate precipitation [17,18]. Enzyme synthesis in bacteria catalyzes the urea reaction to produce ammonia and dissolved inorganic carbon, resulting in alkalinity accumulation near bacterial cells when a calcium source is present.

Carbonate precipitates predominantly form on bacterial cell surfaces and accumulate at particle–particle contacts due to microorganisms' inclination to avoid exposed surfaces and adhere to smaller features [13]. This process enhances cementation at pore throats, leaving larger pores relatively open. While soil stiffness increases with cementation, changes in permeability are minimal, making MICP technology a promising option for internal erosion control. Previous studies [19–26] have highlighted numerous advantages of MICP technology. These benefits include improving soil strength and stiffness, maintaining soil permeability with minimal calcium carbonate precipitation (usually less than 5–6%), providing energy-efficient on-site treatment compared to traditional chemical grouting, and showing rapid biogeochemical reaction rates. However, it is crucial to consider the potential issue of clogging in treated soil, especially in the presence of carbonate content. Feng and Montoya [12] observed that heavily cemented soil by carbonate precipitation (above 3.5%) leads to a significantly non-uniform distribution of precipitation. Lin et al. [27] also found that even low carbonate contents of 1.6% can cause severe uneven distribution of calcite in treated soils. Previous studies have indicated that the effective treatment distance for MICP typically ranges from 0.2 to 1.0 m due to local blockage, which is shorter compared to traditional chemical grouting methods [28]. However, achieving a satisfactory treatment distance with conventional chemical grouting techniques usually requires a substantial amount of energy for injecting or mixing the binder into the soil. This is primarily due to the high viscosity of the conventional binder slurry, particularly at high water/cement ratios. Conversely, the injection of low-viscosity bacterial and cementing solutions has the potential to address this challenge [29,30].

MICP technology effectively combines fine soil particles with coarse particles to reduce erosion potential under seepage [31,32]. It maintains the permeability of the existing soil, preventing significant changes in pore pressure in upstream and downstream areas, thereby

enhancing the overall stability of antifouling barriers. This technology is utilized in both the construction of new antifouling barriers by blending bacteria and cementation solutions with filler materials, and in the emergency repair of existing barriers by injecting bacteria and cement to mitigate ongoing erosion. Current research focuses on erosion control within constructed barriers, with adaptable injection methods proving effective against established barriers. This study aims to (1) investigate the seepage behavior of Zn-contaminated loess, (2) evaluate the feasibility of utilizing MICP for Zn contamination control in loess, and (3) elucidate the enhancement mechanism of Zn-contaminated seepage erosion control through MICP-modified loess.

2. Materials and Methods

2.1. Testing Materials

2.1.1. Tested Soil

The Guanzhong area, located in the middle reaches of the Yellow River, is known as the largest loess region globally, covering approximately 6.4×10^5 km². Soil specimens used in this study were taken from Q₃ loess in Tongchuan City, Shaanxi Province. The disturbed Malan loess specimens were collected from depths of around 3–5 m below the surface and then transported to the laboratory for analysis. The loess displays loose characteristics and a light grayish-yellow color. Particle size analysis was carried out using a Malvern Mastersizer 2000 laser particle size analyzer following pretreatment procedures outlined by Xu et al. [11] and Hou et al. [33]. The physical and mechanical properties of the loess are detailed in Figure 1 and Table 1, in accordance with the Standard for Geotechnical Testing Method [34]. The particle size distribution was obtained using a laser particle size analyzer (WJL-602 Model), indicating that 73.44% of particles were silt, as well as 26.36% clay and 0.20% sand. The liquid limit and plastic limit, tested using a liquid–plastic combine tester, were 33.42% and 20.43%, respectively. Moreover, the plasticity index (value of 13.01%) was the difference between the liquid limit and the plastic limit. The loess is classified as low plasticity clay (CL) according to the ASTM D2487 [35]. Chemical composition analysis of the loess was carried out using inductively coupled plasma mass spectrometry (ICP-MS) as illustrated in Table 2. The primary chemical components identified in the loess specimens are SiO₂, followed by Al₂O₃, CaO, and Fe₂O₃.

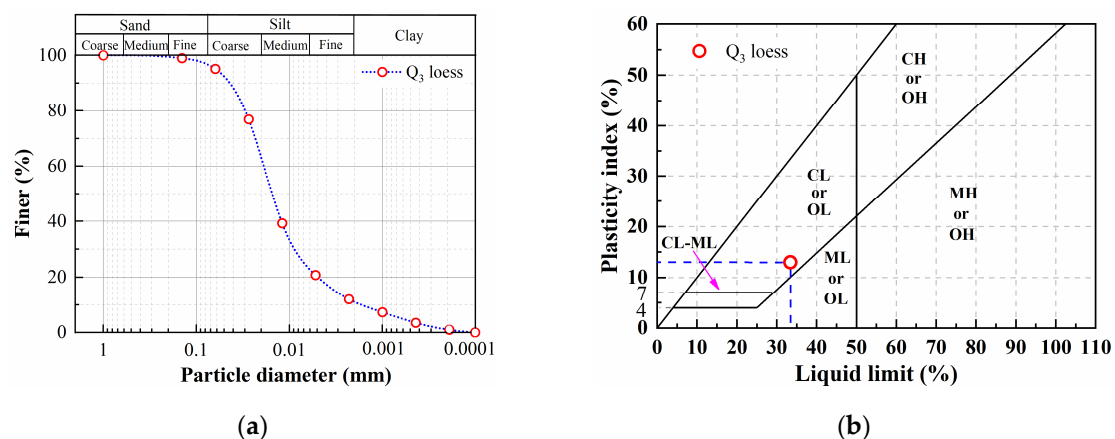


Figure 1. (a) Particle size distribution of Q₃ loess and (b) liquid limit and plastic index.

Table 1. Physicochemical properties of the loess.

Physical Index	Data
Fines (%)	91.18
Sand (%)	8.82
Gravel (%)	0
Specific gravity, G_s	2.72
Void ratio, e	0.88
Dry density, $\rho_{dmax}/(g/cm^3)$	1.78
Initial water content, $w_n/\%$	16.4
The Atterberg limit	
Liquid limit, $wL/\%$	33.42
Plastic limit, $wP/\%$	20.43
Soil classification	CL

Table 2. Chemical element composition of the loess specimen.

Chemical Element	Content (%)
Silicon (Si)	73.66
Aluminum (Al)	15.5
Iron (Fe)	7.93
Potassium (K)	1.09
Magnesium (Mg)	0.95
Sodium (Na)	0.54
Calcium (Ca)	0.33

2.1.2. Bacteria and Cementation Solutions for MICP Treatment

MICP harnesses naturally occurring bacteria to enhance soil mechanical properties by promoting the formation of soil aggregates through calcium carbonate precipitation [31,36,37]. Ureolytic bacteria such as *Bacillus pasteurii*, *Bacillus sphaericus*, *Bacillus licheniformis*, nitrate-reducing bacteria, and other alkaliphilic bacteria are utilized in MICP. *Bacillus pasteurii*, known for its strong tolerance and ease of cultivation, has been shown in previous studies to play a significant role in calcium carbonate precipitation [25,26,31,38,39]. *Sporosarcina pasteurii* (CGMCC1.3687) bacteria were obtained from the China General Microbiological Culture Collection Center for this study. The liquid culture medium consisted of urea (20 g/L), peptone (5 g/L), yeast extract (3 g/L), and manganese sulfate (0.01 g/L) as reported by Jiang et al. [13] and Wang et al. [26]. The pH was adjusted to 7.0 using a 10% NaOH solution and sterilized at 121 °C for 20 min in an autoclave. Following cooling, the bacteria were inoculated at a 1:100 ratio and incubated aerobically in a shaking incubator at 30 °C and 180 rpm for 48 h. Bacterial liquid concentration was determined by OD_{600} at 600 nm wavelength, and urease activity was measured by the average conductivity change within 5 min. The OD_{600} of the cultured liquid was approximately 1.70, with urease activity around 4.0 mM urea hydrolyzed/min, assessed using a spectrophotometer and conductivity meter. Furthermore, the experiment utilized a cementing solution composed of urea and calcium chloride dissolved in deionized water at a 1:1 concentration ratio. Urea functioned as the nitrogen source, while calcium chloride acted as the calcium source in the MICP process [40]. To prevent urea evaporation from the cementing solution over time, it was used within 1 h of preparation.

2.2. Experimental Methods

2.2.1. Specimen Preparation

The susceptibility of natural loess to uncontrollable factors, such as root and insect holes, poses challenges in maintaining specimen consistency during collection, thereby impacting the reliability of research outcomes. To overcome this challenge, we employed the wet compaction method to create loess specimens with optimal moisture content (see Figure 2). To compare, initial infiltration tests were conducted using deionized water and

ZnCl₂ solution on untreated specimens. The process of MICP treatment for loess specimens consists of two stages: (1) injection of bacterial solution and (2) injection of cementing solution. As highlighted by Jiang et al. [13], excessively high or frequent injection rates may result in precipitation flushing, thus affecting precipitation efficiency. Hence, we established the injection rate of bacterial solution at 2 mL/min and the injection rate of cementing solution at 4 mL/min.

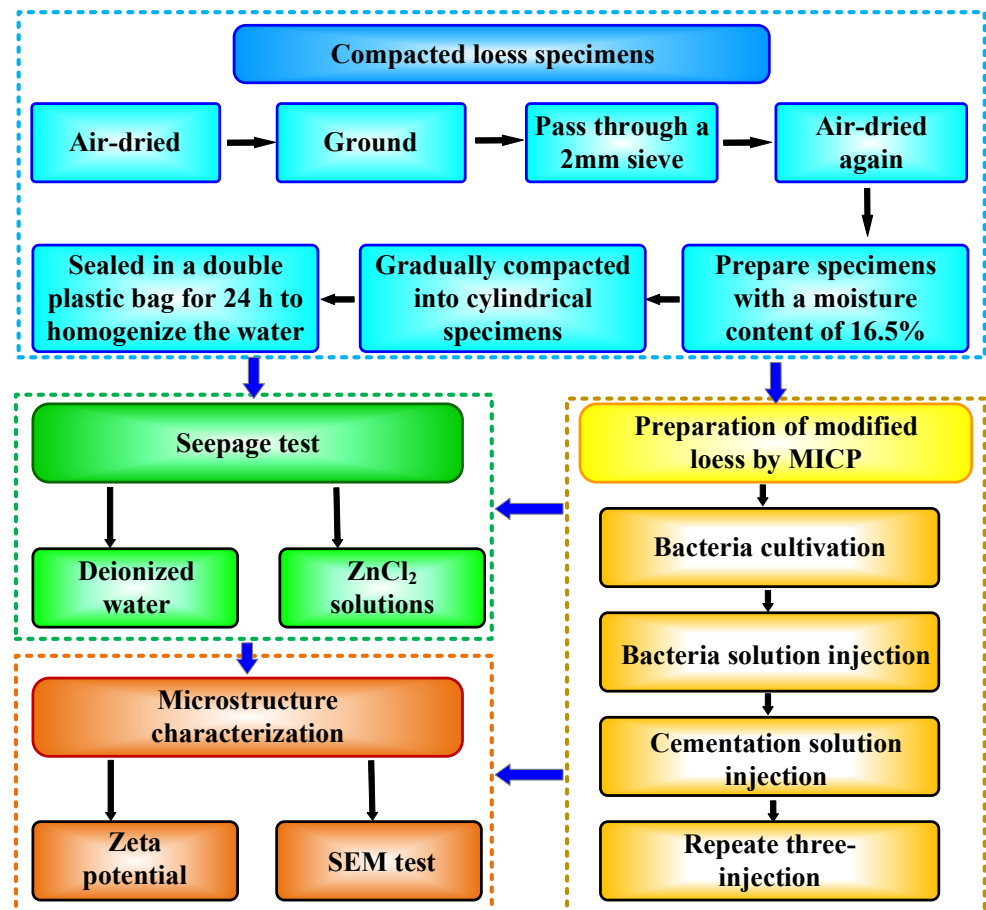


Figure 2. The procedures for experimental methods.

Despite the limitations of working with small specimen sizes in laboratory testing, which may not fully represent real soil conditions, this issue can be mitigated by using parallel specimens. Laboratory methods are generally deemed more dependable due to the controlled settings in which they are carried out, including temperature and hydraulic gradients. Additionally, soil specimen permeability is typically assessed in the laboratory under constant load, as shown in Figure 3 for saturated hydraulic conductivity testing. In our research, we employed the Chinese ST-55 permeameter and utilized the constant head method to measure permeability. The required hydraulic gradient was established by adjusting the water tank's height, and outflow measurements were taken only after the hydraulic head had stabilized. The infiltration test on loess closely followed the procedures outlined by Xu et al. [8,11].

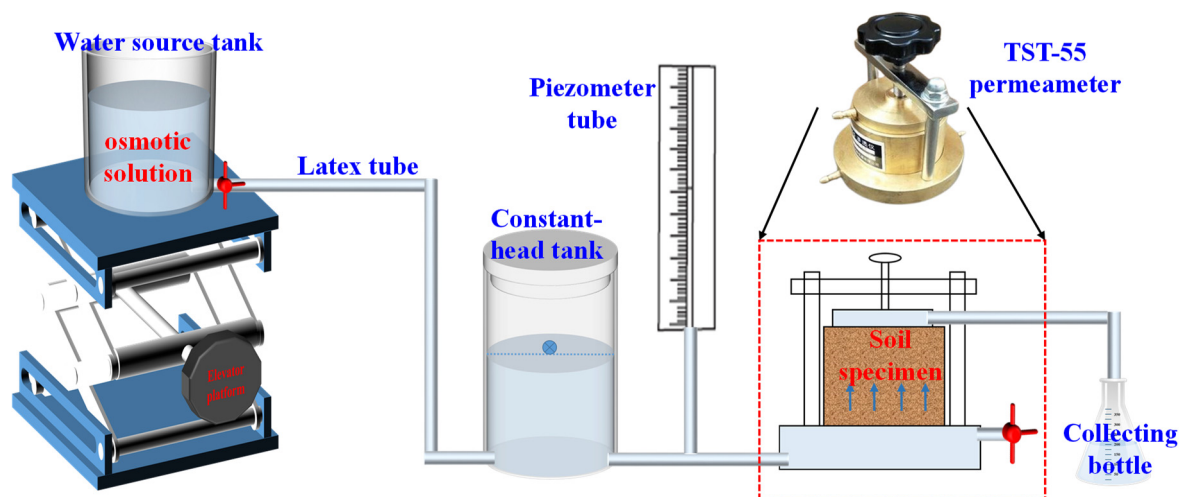


Figure 3. Schematic diagram of seepage test device.

2.2.2. Zn-Contaminated Solutions

The Guanzhong Plain, a typical agricultural area in China, has seen an increase in zinc contamination in its loess due to rapid agricultural and industrial development in the NW region. Zinc (Zn), a trace element essential for plant growth, plays a central role in this issue. To investigate the geochemical mechanisms of soil microstructure evolution and percolation behavior under Zn^{2+} erosion, we employed $ZnCl_2$ reagents known for their high solubility. Previous studies have indicated that a concentration of 2.5 mmol/L of inorganic salt solution can effectively illustrate the influence of ion types on the structure and percolation behavior of loess [13]. Consequently, solid powder reagents were dissolved in deionized water (DW) to create a 2.5 mmol/L concentration of contaminated solution. Furthermore, DW served as the control group in the experiment.

2.2.3. Seepage Tests

Although the drawback of laboratory testing may suffer from small sample sizes that may not fully represent the actual soil medium, this limitation can be addressed by using parallel specimens. Laboratory methods are generally considered more reliable due to their controlled environments, including temperature and hydraulic gradients. The measurement of soil specimen permeability is commonly conducted in the laboratory under constant loading conditions, as shown in Figure 3 for saturated hydraulic conductivity testing. In this study, the Chinese ST-55 permeability meter was used to determine permeability through the constant head method. The necessary hydraulic gradient was achieved by adjusting the water tank's height, and outflow data were collected once the hydraulic head had stabilized. The procedures for the loess infiltration tests closely followed those outlined by Xu et al. [8]. All tests applied to the present work had three replicates, and the statistical analysis indicated that the coefficient of variance was far below 10%. Results from the three test trials were averaged.

2.2.4. Zeta Potential Measurement

Charged soil particles in aqueous solution can attract ions with opposite charges, forming stable connections in a Stern layer close to the particles. Further away, in the diffuse layer, weaker adsorption forces create looser connections. The concentration of Na^+ , K^+ , Ca^{2+} , and Mg^{2+} ions was measured via ion chromatography (IC) (Thermo Fisher Scientific, Fair Lawn, NJ, USA) every 12 h during DW and $ZnCl_2$ seepage tests. Heavy metal ions can alter the thickness of DDL by adsorbing onto clay mineral surfaces through hydration and ion exchange reactions, impacting soil structure and hydraulic properties. Zeta potential analysis can characterize the thickness of DDL. Prior to experimentation, loess was sieved through a 50 μm sieve, then treated with different chemical solutions and

stirred for 30 min. Zeta values of loess particles in various heavy metal solutions were determined using a Zeta potential analyzer (Zeta Plus, Malvern, UK). DW was used to rinse the microelectrophoresis cell before and after each measurement to prevent contamination.

2.2.5. Microstructure Characterization

Scanning electron microscopy (SEM) is a widely used technique for analyzing soil microstructures, allowing for both qualitative and quantitative assessments. In this study, we utilized field emission SEM (Zeiss Gemini sigma 300, Oberkochen, Germany) to investigate the microstructure of loess specimens before and after seepage to understand the seepage characteristics and mechanisms of heavy metal-contaminated loess. The methodology for characterizing soil microstructures in our research was adapted from previous studies by Xu et al. [11] and Hou et al. [33]. Specimens were trimmed to create films measuring 2 mm in height, 5 mm in width, and 5 mm in length. These films were dried at 60 °C and reinforced with a solidification agent. Subsequently, they were ground with sandpaper, polished with an alumina solution to emphasize microstructural features, and finally coated with gold foil before being installed. Our SEM analysis revealed notable variations in the microstructural features of loess at different magnifications, as depicted in Figure 4. Therefore, we opted for a magnification of 1000× to examine the evolution of loess microstructures under Zn²⁺ seepage, drawing inspiration from the work of Li et al. [17]. ImagePro Plus 6.0 (IPP 6.0) software was employed for preprocessing, segmentation, and parameter extraction of the SEM images. By following the pore classification criteria established by Lei et al. [41], we calculated the area ratio of each pore.

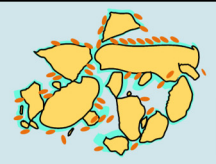
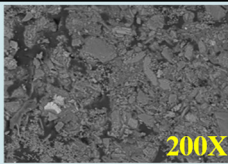
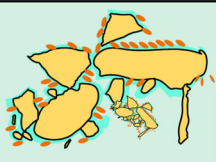
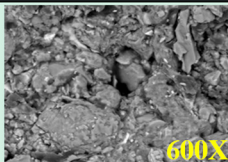
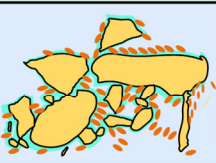
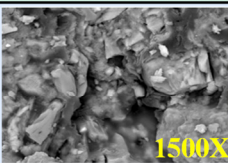
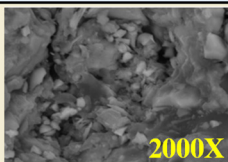
Magnification	Typical microstructure	Associated SEM images	Feature description
Low times ($X \leq 200$)			The observation range is wide. The overall information of the sample can be observed, while the details cannot be obtained.
Medium times ($200 < X \leq 1000$)			The observation range is medium. The degree of cementation can be basically recognized, while the contact relationship between particles is ambiguous.
High times ($1000 < X \leq 4000$)			The observation range is small. The particle skeleton shape, contact relationship, pore type and cementation degree are clearly visible.
Extra high times ($1000 < X \leq 4000$)			The observation range is very small, which is only suitable for single point observation, and the overall information of microstructure cannot be obtained.

Figure 4. SEM image features under different magnifications.

3. Results

3.1. Seepage Behavior of Loess

A thorough understanding of soil hydraulic conductivity is crucial for studying permeability behavior. Darcy's law offers insights into the temporal variations and statistical characteristics of permeability in compacted loess. In the case of DW seepage, the permeability of compacted loess gradually increases over time, with an initial rapid decrease in the first three days of the seepage test, followed by a more gradual decline (see Figure 5).

The concentrations of Ca^{2+} , Mg^{2+} , Na^+ , and K^+ ions also fluctuate during the seepage test, with Na^+ exhibiting the most significant changes initially, followed by Ca^{2+} . In subsequent seepage tests, both Na^+ and Ca^{2+} concentrations decrease, while Mg^{2+} and K^+ concentrations remain relatively stable (see Figure 6). When seeped with a ZnCl_2 solution, the permeability of compacted loess increases over time, indicating a notable influence of Zn^{2+} on loess seepage behavior. The experimental process shows a slight increase in Mg^{2+} concentration over time, while the concentration of Ca^{2+} demonstrates a significant upward trend. Exposure of calcite to ZnCl_2 seepage leads to the formation of calcium bicarbonate and magnesium bicarbonate, subsequently reducing the ionization of calcium and magnesium ions. In comparison to the compacted loess specimen under DW seepage, the permeability of the loess specimen under ZnCl_2 solution seepage exhibits a noticeable change, increasing by 554.5%.

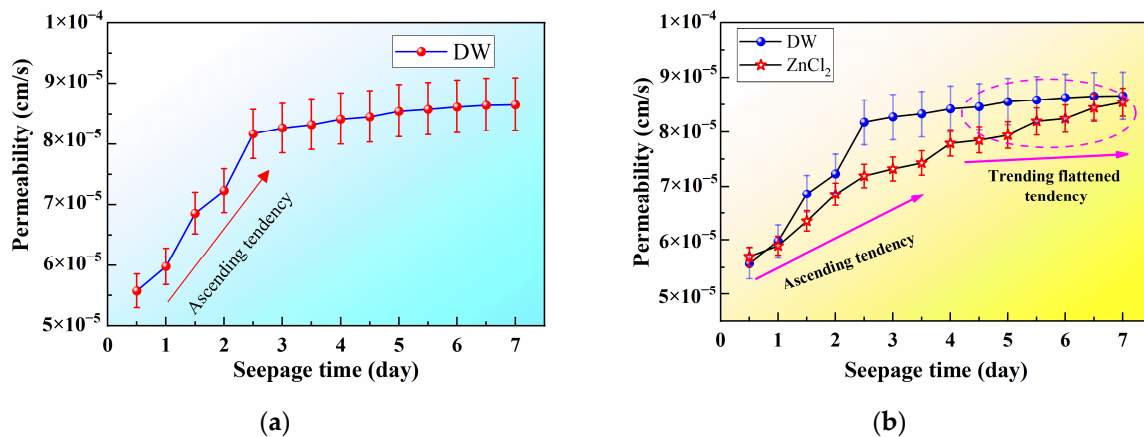


Figure 5. Temporal relationship of permeability versus seepage time for the seepage test: (a) deionized water and (b) deionized water and ZnCl_2 solutions.

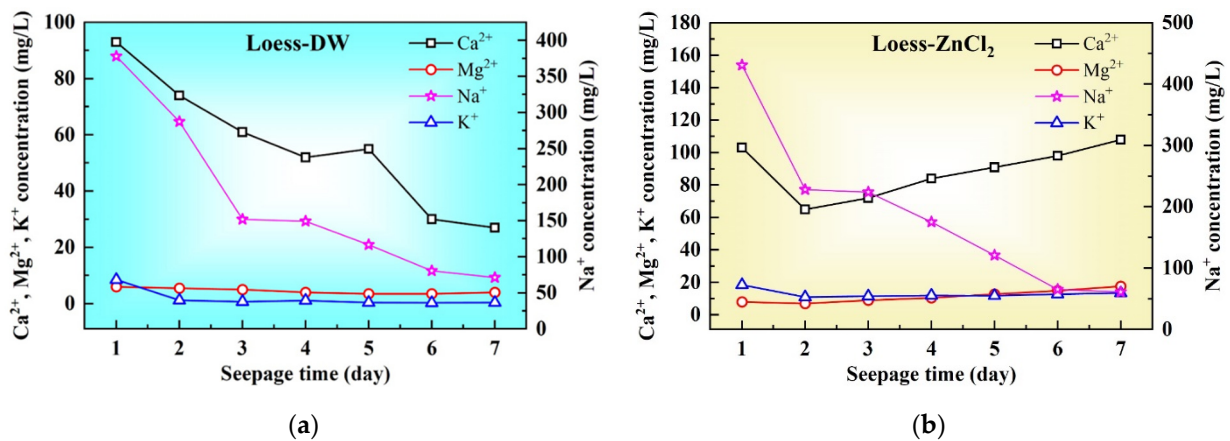


Figure 6. Temporal relationship of cation ion concentration versus seepage time for the seepage test of loess: (a) DW and (b) ZnCl_2 solutions.

3.2. Seepage Behavior of Modified Loess

To investigate the impact of MICP technology on loess under the seepage of DW and ZnCl_2 solution, seepage tests were conducted on untreated and modified loess specimens. The evolution of permeability over time was compared, as shown in Figure 7. When exposed to DW seepage, the permeability of loess gradually increases while the leaching of various ions decreases, indicating a weakening of geochemical processes. In contrast, under ZnCl_2 solution seepage, the permeability of compacted loess increases over time. MICP treatment significantly reduces the permeability of loess under DW seepage conditions by solidifying the specimens with calcium carbonate, filling the pores between soil parti-

cles and strengthening the bonding effect. However, under ZnCl_2 solution seepage, the permeability of modified loess increases gradually due to the hydrolysis of Zn^{2+} creating an acidic environment that promotes the dissolution of carbonate minerals and MICP mineralization products in loess. This process, particularly the variations in ion concentrations such as Na^+ , Mg^{2+} , and K^+ , as depicted in Figure 8, highlights significant chemical interactions between loess and modified loess induced by ZnCl_2 solution. Additionally, the adsorption of Zn^{2+} and its DDL effect compress the diffusion layer, enhancing the presence of free water channels. The increase in seepage time leads to a gradual increase in the permeability coefficient, as supported by Chen et al. [42]. Furthermore, studies by Jiang et al. [13], Huang et al. [36], Xing et al. [37], Kang et al. [38], Li et al. [39], and Wang et al. [25] suggest that carbonate precipitation enhances particle bridging through the adsorption/encapsulation of sand–clay mixtures, thereby enhancing erosion resistance. The use of MICP technology in this study has shown a significant reduction in the permeability coefficient (see Figure 7). However, as leaching time extends, there is a gradual increase in zinc content, which inhibits mineralization reactions and results in a gradual increase in the permeability coefficient. This finding aligns with the research findings of Wang et al. [43].

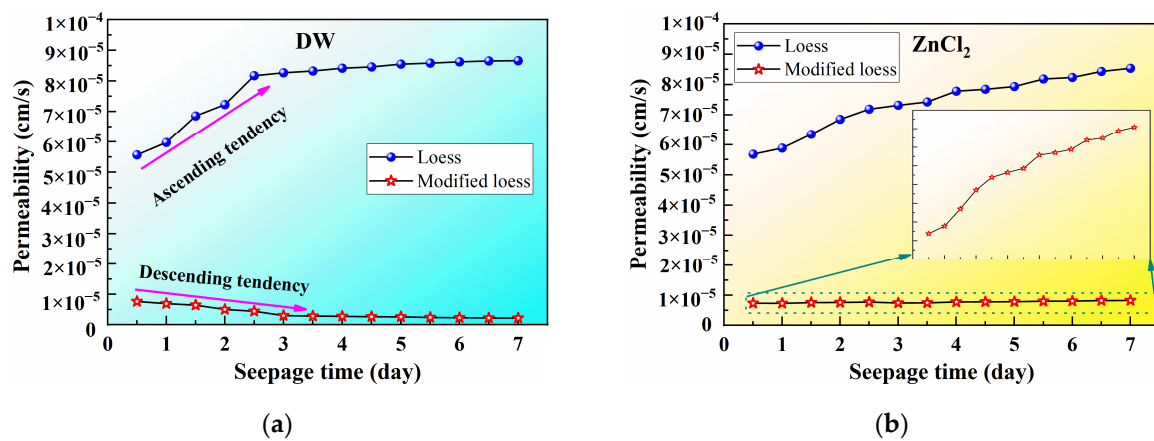


Figure 7. Temporal relationship of permeability versus seepage time for the seepage test of loess and modified loess: (a) DW and (b) ZnCl_2 solutions.

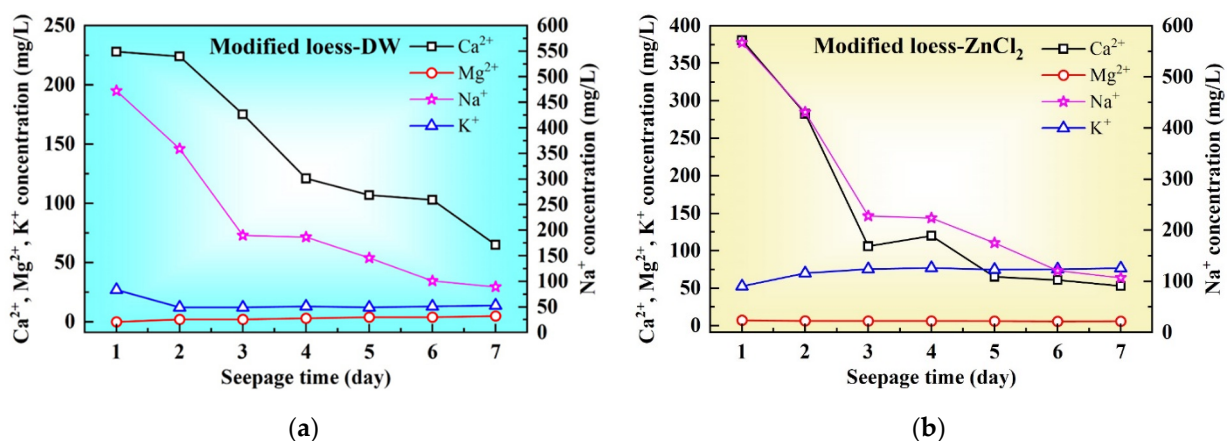


Figure 8. Temporal relationship of cation ion concentration versus seepage time for the seepage test of modified loess: (a) DW and (b) ZnCl_2 solutions.

3.3. Microstructural Characteristics

Particle morphology, contact relationships, pore structure, and degree of cementation collectively determine the microstructure of soil, thereby influencing its macroscopic physical and mechanical properties [11,25]. Figure 9 provides an overview of the microstructure

of compacted loess and modified loess under the seepage of DW and ZnCl₂ solutions. Before seepage test, the outlines of coarse particles in compacted loess are clearly visible, with a small amount of fine particles covering them. The particle distribution in the loess specimens is uniform, and the microstructure is relatively dense. However, pore development is incomplete, and particles form an interlocking structure. The primary contact mode between particles is embedded contact, followed by aerial contact. Following DW seepage, some coarse particles become covered by fine particle aggregates, forming larger aggregates that enhance the development of pore space. This phenomenon is more pronounced in loess specimens infiltrated with ZnCl₂ solutions, where pore space develops more effectively, leading to a significant increase in the permeability of loess under the seepage of ZnCl₂ solutions over time. While aggregates are present in samples of MICP-modified loess after DW seepage, they appear rough, indicating differences in microstructural characteristics compared to after ZnCl₂ seepage. This is primarily attributed to an increase in van der Waals forces and a decrease in electrostatic repulsion during seepage. The formation of large aggregates is more prominent in loess specimens contaminated with Zn²⁺, where the aggregates are larger, and the flocculation and expansion of pore space are more noticeable. This could lead to increased permeability and reduced impermeability. These findings suggest that the introduction of Zn²⁺ lead to the reorganization of soil microstructure, negatively impacting the engineering performance of loess. However, MICP-modified loess remains an effective treatment method. Compared with the modified loess specimen under DW seepage, the permeability of loess specimen under ZnCl₂ solution seepage exhibits an obvious change, increasing by 1450%.

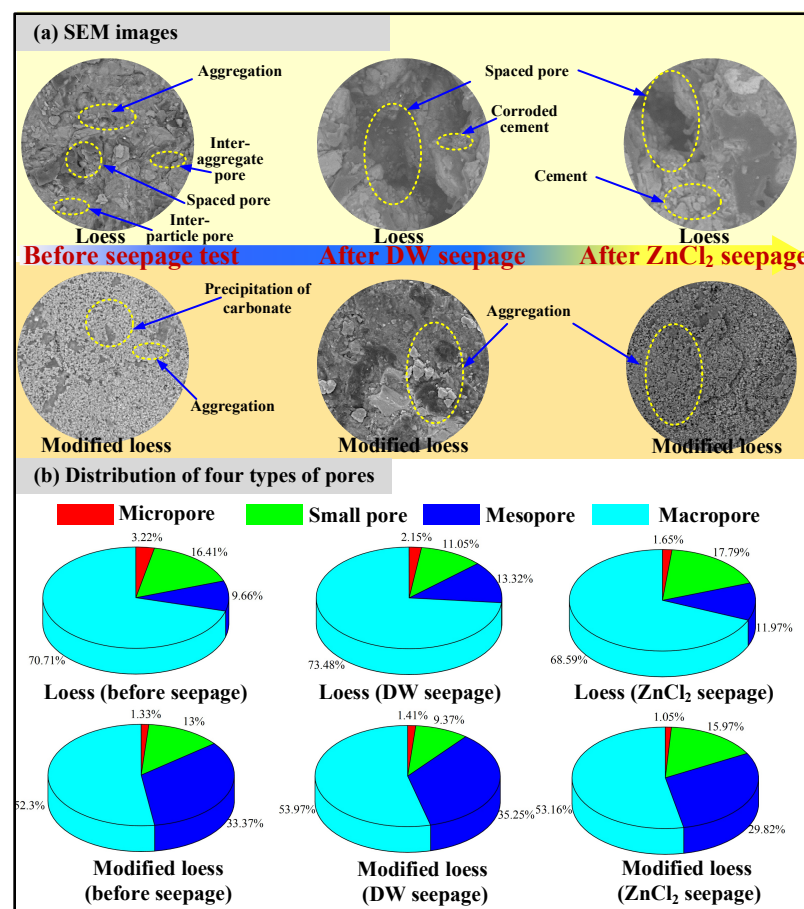


Figure 9. (a) Distribution and (b) area proportion of four types of pores in loess and modified loess.

Compared to the compacted natural loess specimens, the changes in micropore area ratio after DW and ZnCl_2 seepage were minimal, decreasing by 1.07% and 1.57%, respectively. After DW seepage, there was a reduction in the proportion of small pore area while the proportions of medium and large pore areas increased. This shift from micropores and small pores to medium and large pores during DW seepage led to a gradual increase in permeability. Conversely, with the seepage of the ZnCl_2 solutions, the changes in micropore area ratio were more pronounced, decreasing by 48.80%, with an increase in mesopore areas by 23.9%. The decrease in permeability can be primarily attributed to the transition from small pores to medium pores, positively impacting permeability [8]. This suggests that variations in permeability characteristics between DW seepage and ZnCl_2 solution seepage are mainly influenced by mesopores. Additionally, the soil skeleton particle area ratio experienced the most significant decrease in Zn-contaminated loess, while the total pore area ratio increased the most, indicating substantial geochemical interactions between water and loess during the seepage process.

4. Discussion

4.1. DDL Effect

The presence of heavy metals in soils with clay minerals, such as those found in loess, can result in cation exchange and adsorption processes. This can potentially lead to higher leaching ion concentrations, changes in soil strength, and alterations in soil microstructure [44–47]. It is essential to account for these effects when conducting infiltration experiments in zinc and copper-contaminated loess. The introduction of Zn^{2+} disrupts the charge equilibrium of clay minerals, causing the adsorption of ions like Na^+ , K^+ , Ca^{2+} , and Mg^{2+} on the surfaces of clay minerals. This results in cation exchange and an increase in leachate ion concentration, as illustrated in Figure 6. Furthermore, heavy metal ions in the exchange phase may decrease the thickness of the double layer, leading to clay particle flocculation and an increase in pore space [48–50]. Additionally, when clay content exceeds 10%, the double layer effect becomes significant [7]. This has implications for the shrinkage rate of clay aggregates due to heavy metal leaching through infiltration. Similar effects have been observed in other heavy metal-contaminated soils, corroborating the broader relevance of the study's findings [32,44,45]. Zeta potential analysis can be used to evaluate the thickness of the double layer, with positive values in the loess indicating the entry of Ca^{2+} and Zn^{2+} into the Stern layer through electrostatic attraction, leading to a change in Zeta potential sign (see Figure 10) [48,51]. The Zeta potential values of the loess in DW and ZnCl_2 solutions were positive, suggesting the entry of Ca^{2+} and Zn^{2+} into the Stern layer through electrostatic attraction, resulting in a change in Zeta potential value [8]. Furthermore, heavy metal ions form inner-layer complexes after being adsorbed by particles, exerting a strong compressive effect on the diffusion layer and causing expansion in the free layer. According to the double-layer theory, the free gravitational water space of Zn-contaminated loess increases, thus enhancing the permeability of the loess [48,51].

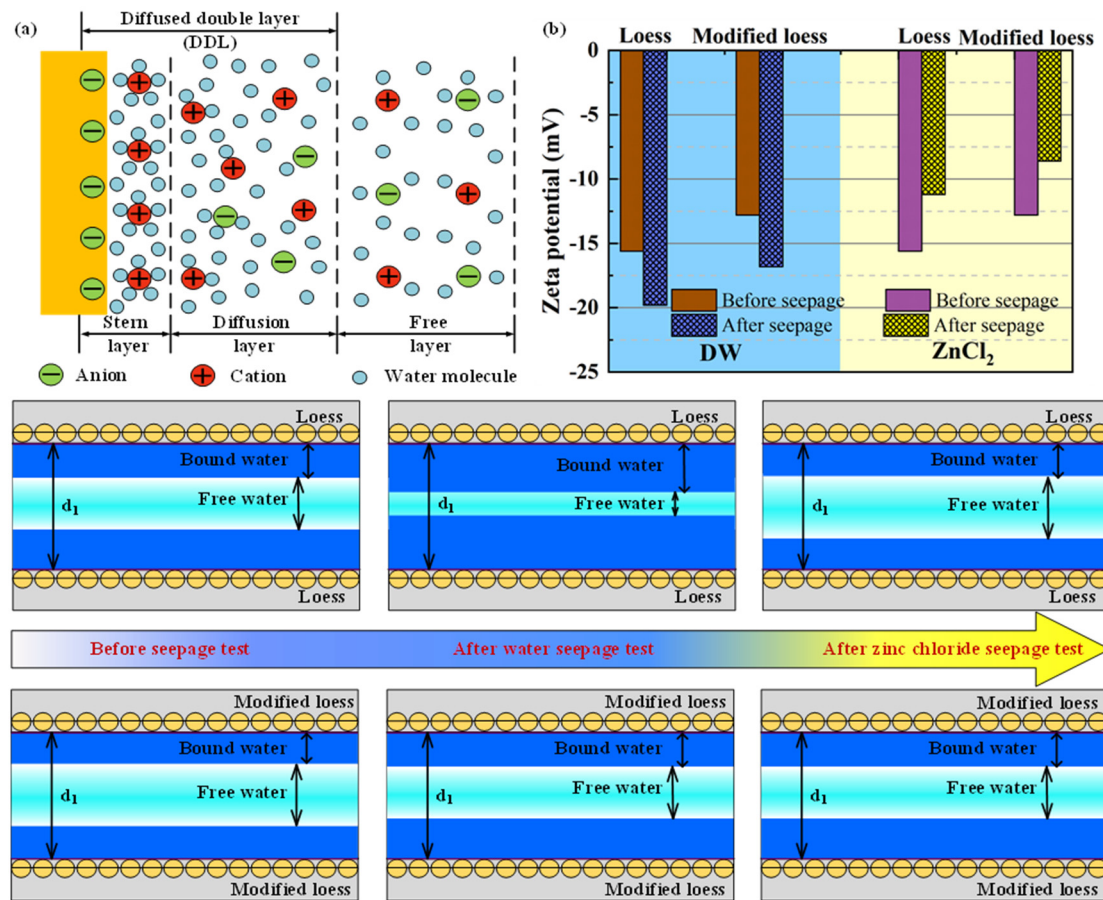


Figure 10. (a) Schematic illustration of the diffuse double layer model, (b) variation of the zeta potential and diffuse double layer before and after seepage test.

4.2. Response Mechanism of Seepage Behavior

Based on the geochemical interactions and morphological characteristics of loess microstructure discussed earlier, schematic diagrams illustrating the evolution of loess microstructure under varying infiltration conditions are presented in Figure 11. At optimal moisture content, a water film surrounds particle surfaces, facilitating particle aggregation and the formation of a relatively stable structure (Figure 10a) [11]. During DW seepage, erosion enhances pore connectivity, and cation exchange between Ca^{2+} and Na^+ results in the formation of particle aggregates, creating pathways for water flow [2,11]. Additionally, the DDL thickness on clay particle surfaces increases, as depicted in Figure 10b. Consequently, although the saturated hydraulic conductivity of compacted loess exhibits a rising trend, the increment is only 7.7% (Figure 11a). A rapid growth phase is observed in the final 4 days of the seepage cycle, possibly attributed to carbonate dissolution in the loess [49]. Other studies suggest that carbonate dissolution significantly contributes to enhancing water channels within loess [8,52]. When utilizing ZnCl_2 solution for seepage, the hydrolysis of Zn^{2+} results in the release of abundant free hydrogen ions. The intricate chemical reactions of hydrogen ions with calcium and magnesium compounds present in loess diminish the level of soil cementation [51]. Meanwhile, the alternate adsorption of Zn^{2+} and its double layer effect not only strongly promote particle aggregation but also compress the diffusion layer, increasing the abundance of free water channels (Figure 10b). As a result, the saturated hydraulic conductivity of loess exhibits a significant increasing trend. The application of MICP technology notably reduces the pores in compacted loess, leading to the formation of a calcium carbonate hard shell layer. This layer is characterized by a uniform texture, dense surface, and substantial thickness, covering the soil surface, as shown in Figure 11. The water-resistant hard-shell layer possesses a certain level of strength,

effectively preventing moisture from penetrating the specimen and causing corrosion. At a macroscopic level, the specimen demonstrates a low permeability coefficient and strong erosion resistance, consistent with previous test results (see Figure 11) [48–51].

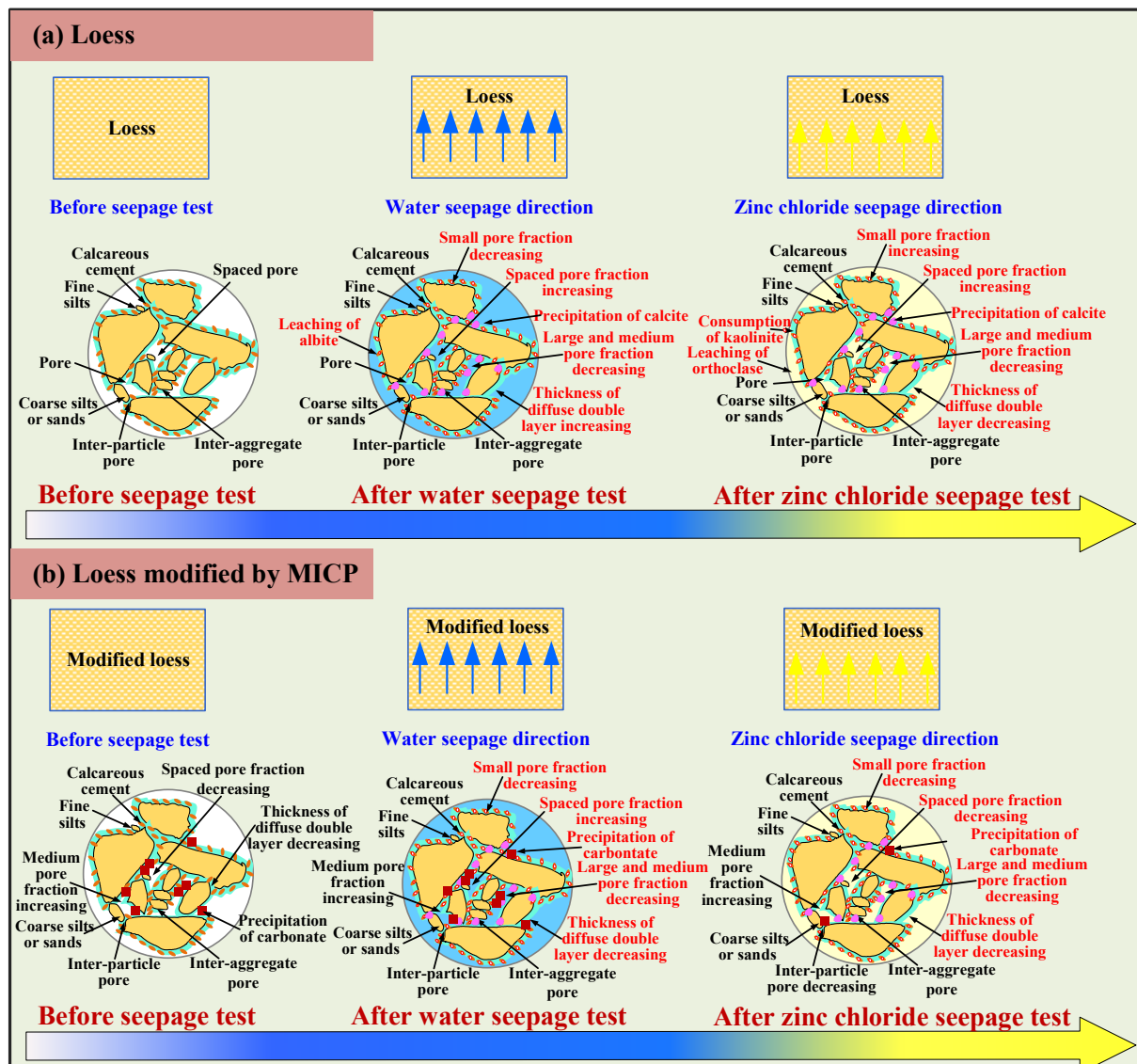


Figure 11. Schematical illustration of the loess microstructure before and after seepage test.

MICP technology plays a crucial role in reducing internal erosion and soil permeability by inducing the precipitation of carbonate minerals. This process involves two key mechanisms: absorbing and encapsulating fine particles with a high surface area, and bridging contacts between coarse particles to enhance soil stiffness. The former helps in retaining fine particles, while the latter minimizes soil shrinkage. Consequently, loess treated with MICP exhibits improved erosion resistance, optimizing its structure and enhancing its ability to resist the seepage of DW and $ZnCl_2$ solutions. The permeability of the soil is significantly decreased, as demonstrated in Figures 5 and 7. Moreover, the influence of seepage time on the permeability coefficient diminishes over time. These results indicate that MICP technology holds great promise for soil and water conservation, as well as geological disaster prevention in the Loess Plateau. Previous studies by Jiang et al. [13], Huang et al. [36], Xing et al. [37], Kang et al. [38], Li et al. [39], and Wang et al. [25] have highlighted that carbonate precipitation enhances particle bridging by adsorbing/encapsulating sand–clay mixtures, thereby boosting erosion resistance. The application of MICP technology in

this study has led to a notable decrease in the permeability coefficient. However, with prolonged leaching time, there is a gradual rise in zinc content, hindering mineralization reactions and causing a gradual increase in the permeability coefficient. This observation is in line with the findings of Wang et al. [42]. Further work on the statistical analysis, Zeta test results against loess contaminated with Zn^{2+} and the change in shear strength of loess contaminated with Zn^{2+} under different coaxial loads is still ongoing and the results will be discussed in another paper.

5. Conclusions

This study identified the permeability, leaching characteristics, and microstructure evolution of loess and modified loess under DW and $ZnCl_2$ seepages. The geochemical mechanism driving the seepage behavior was also revealed. Overall, the results and discussion led to some main conclusions:

(1) Among the various cations leaching out, the most significant concentration variation over time was observed for Na^+ ions during the early stage of DW seepage. Under DW seepage, the concentration of Na^+ exhibited a decreasing trend. The penetration of Na^+ in loess into the double layer increased the Zeta potential, causing repulsion to exceed attraction, leading to the expansion and dispersion of clay particles in loess and the formation of small pores at the junction of loess particles. Additionally, as seepage time extended, the permeability coefficient gradually increased.

(2) The hydrolysis of Zn^{2+} resulted in an acidic pore water environment, which facilitated the dissolution of carbonate minerals in loess. The alternating adsorption of Zn^{2+} and its DDL effect reduced the thickness of the diffusion layer, enhancing the attraction between soil particles, minimizing repulsion, and strongly promoting the formation of particle aggregation structure. Moreover, the proportion of small and medium pores contaminated by Zn^{2+} in loess increased, indicating significant geochemical processes occurring during the seepage.

(3) Compared to natural loess, MICP-modified loess shows a significant decrease in permeability coefficients to both DW and $ZnCl_2$. This is because MICP modified loess particles by producing a large number of calcium carbonate crystals, which fill the pores of loess and stack on the loess skeleton to form cementation. The formation of the cementation structure reduces macropores and micropores, decreasing the ability of water infiltration, leading to a significant decrease in permeability coefficients. On the other hand, the carbonate formed by MICP technology can resist the increase in Zeta potential, maintaining the stability of the aggregation structure under infiltration.

(4) The above research results and discussions are of great theoretical significance for revealing the geochemical processes of Zn erosion in loess and the infiltration response mechanism of MICP-modified loess. The findings of this study have important practical significance for the prevention and control of geological disasters in the loess plateau region for engineering construction. In future research, further investigation should be conducted on the permeation evolution, heavy metal blocking capacity, and microstructural characteristics of MICP-modified loess under heavy metal seepage conditions. Further research on the above shortcomings is underway, and the results will be presented in another document.

Author Contributions: P.H.: Investigation, formal analysis, writing—reviewing and editing. J.G.: Investigation, formal analysis, writing—reviewing and editing. S.Z.: Conceptualization, methodology, resources, writing—original draft preparation. All authors have read and agreed to the published version of the manuscript.

Funding: This research received no external funding.

Data Availability Statement: The data used to support the findings of this study are available from the corresponding author upon request.

Conflicts of Interest: All the authors have read and approved this version of the article, and due care has been taken to ensure the integrity of the work. I would like to declare on behalf of my co-authors that the work described was original research that has not been published previously, and not under consideration for publication elsewhere, in whole or in part. We declare that all authors have no any actual or potential conflicts of interest including financial, personal or other relationships with other people or organizations.

References

1. Chen, Y.; Wang, C.Q.; Jiang, S.X.; Luo, L.J.; Li, X.; Chen, H.; Zheng, J.R.; Jia, W. Idation effect and anti-rainfall erosion of microbially induced carbonate precipitation on abandoned soil of transmission tower. *Sci. Technol. Eng.* **2023**, *23*, 14713–14720. (In Chinese)
2. Lu, T.; Tang, Y.M.; Tie, Y.B.; Hong, B.; Feng, W. Fractal analysis of small-micro pores and estimation of permeability of loess using mercury intrusion porosimetry. *J. Zhejiang Univ.-Sci. A (Appl. Phys. Eng.)* **2023**, *7*, 584–595. [[CrossRef](#)]
3. Zhang, Q.Y.; Qian, H.; Xu, P.P.; Hou, K.; Zhang, Y.T.; Qu, W.G.; Lin, T.; Chen, Y. Microscale evidence for and formation mechanisms of shear-strength anisotropy of a loess-paleosol sequence since the late Early Pleistocene: The case study of the Xiushidu profile, Southern Chinese loess Plateau. *Catena* **2022**, *213*, 106228. [[CrossRef](#)]
4. Adimalla, N. Heavy metals pollution assessment and its associated human health risk evaluation of urban soils from Indian cities: A review. *Environ. Geochem. Health* **2020**, *42*, 173–190. [[CrossRef](#)] [[PubMed](#)]
5. Zhang, S.Q.; Zhang, X.; Zhang, K.N.; Yuan, B.Y.; Ren, D.J.; Zhang, X.Q. Comparison of remediation mechanism of heavy metal-contaminated soil by combined leaching and two-step leaching. *Water Air Soil Pollut.* **2023**, *234*, 387. [[CrossRef](#)]
6. Wu, Y.; Pan, Z.; Zhu, C.; Ding, S.; Zhang, Z.; Hu, K. Research progress on engineering properties of heavy metal contaminated soil. *J. Henan Univ. (Nat. Sci.)* **2020**, *50*, 750–756.
7. Gajo, A.; Maines, M. Mechanical effects of aqueous solutions of inorganic acids and bases on a natural active clay. *Geotechnique* **2007**, *8*, 687–699. [[CrossRef](#)]
8. Xu, P.P.; Qian, H.; Li, W.Q.; Ren, W.H.; Yang, F.X.; Wang, L.B. New insights into the seepage behavior of heavy metal-contaminated loess and its underlying geochemical mechanism. *J. Hydrol.* **2023**, *620*, 129476. [[CrossRef](#)]
9. Zeng, X.Y.; Li, S.W.; Leng, Y.; Kang, X.H. Structural and functional responses of bacterial and fungal communities to multiple heavy metal exposure in arid loess. *Sci. Total Environ.* **2020**, *723*, 138081. [[CrossRef](#)] [[PubMed](#)]
10. Liu, Y.H.; Ren, X. Solidification, repair and long-term stability analysis of heavy metal contaminated soil on Zhongchuan railway. *Fresenius Environ. Bull.* **2021**, *30*, 2193–2200.
11. Xu, P.P.; Zhang, Q.Y.; Qian, H.; Li, M.N.; Yang, F.X. An investigation into the relationship between saturated permeability and microstructure of remolded loess: A case study from Chinese Loess Plateau. *Geoderma* **2021**, *382*, 114774. [[CrossRef](#)]
12. Feng, K.; Montoya, B.M. Influence of confinement and cementation level on the behavior of microbial-induced calcite precipitated sands under monotonic drained loading. *J. Geotech. Geoenviron. Eng.* **2016**, *142*, 04015057. [[CrossRef](#)]
13. Jiang, N.J.; Soga, K.; Kuo, M. Microbially induced carbonate precipitation for seepage-induced internal erosion control in sand-clay mixtures. *J. Geotech. Geoenviron. Eng.* **2017**, *143*, 04016100. [[CrossRef](#)]
14. Wen, K.; Li, Y.; Liu, S.; Bu, C.; Li, L. Development of an improved immersing method to enhance microbial induced calcite precipitation treated sandy soil through multiple treatments in low cementation media concentration. *Geotech. Geol. Eng.* **2019**, *37*, 1015–1027. [[CrossRef](#)]
15. Choi, S.G.; Chang, I.; Lee, M.; Lee, J.H.; Han, J.T.; Kwon, T.H. Review on geotechnical engineering properties of sands treated by microbially induced calcium carbonate precipitation (MICP) and biopolymers. *Constr. Build. Mater.* **2020**, *246*, 118415. [[CrossRef](#)]
16. Safaa, M.E. A critical review of microbially induced carbonate precipitation for soil stabilization: The global experiences and future prospective. *Pedosphere* **2023**, *5*, 717–730.
17. Li, M.D.; Wen, K.J.; Li, Y.; Zhu, L.P. Impact of oxygen availability on microbially induced calcite precipitation (MICP) treatment. *Geomicrobiol. J.* **2018**, *35*, 15–22. [[CrossRef](#)]
18. Liu, S.Y.; Wang, R.K.; Yu, J.; Peng, X.Q.; Cai, Y.Y.; Tu, B.X. Effectiveness of the anti-erosion of an MICP coating on the surfaces of ancient clay roof tiles. *Constr. Build. Mater.* **2020**, *243*, 118202. [[CrossRef](#)]
19. Qabany, A.A.; Soga, K. Effect of chemical treatment used in MICP on engineering properties of cemented soils. *Geotechnique* **2013**, *63*, 331–339. [[CrossRef](#)]
20. Wang, Y.Z.; Konstantinou, C.; Soga, K.; Biscontion, G.; Kabla, A.J. Use of microfluidic experiments to optimize MICP treatment protocols for effective strength enhancement of MICP-treated sandy soils. *Acta Geotech.* **2022**, *17*, 3817–3838. [[CrossRef](#)]
21. Su, F.; Yang, Y.Y.; Qi, Y.; Zhang, H.N. Combining microbially induced calcite precipitation (MICP) with zeolite: A new technique to reduce ammonia emission and enhance soil treatment ability of MICP technology. *J. Environ. Chem. Eng.* **2022**, *10*, 107770. [[CrossRef](#)]
22. Kulkarni, P.B.; Nemade, P.D. Improvement of strength of locally available soils using microbial induced calcite precipitation. *Int. J. Recent Technol. Eng.* **2019**, *8*, 219–224. [[CrossRef](#)]
23. Wang, Y.J.; Jiang, N.J.; Saracho, A.C.; Doygun, O.; Du, Y.J.; Han, X.L. Compressibility characteristics of bio-cemented calcareous sand treated through the bio-stimulation approach. *J. Rock Mech. Geotech. Eng.* **2023**, *2*, 510–522. [[CrossRef](#)]

24. Wang, Y.N.; Li, S.K.; Li, Z.Y.; Garg, A. Exploring the application of the MICP technique for the suppression of erosion in granite residual soil in Shantou using a rainfall erosion simulator. *Acta Geotech.* **2023**, *18*, 3273–3285. [[CrossRef](#)]
25. Wang, S.; Fang, L.; Dapaah, M.F.; Niu, Q.; Cheng, L. Bio-remediation of heavy metal-contaminated soil by microbial-induced carbonate precipitation (MICP)-A critical review. *Sustainability* **2023**, *17*, 7622. [[CrossRef](#)]
26. Wang, J.; Long, Y.; Zhao, Y.; Pan, W.; Qu, J.; Yang, T.; Huang, X.; Liu, X.; Xu, N. Numerical simulation of forming MICP horizontal seepage reducing body in confined aquifer for deep excavation. *Appl. Sci.* **2023**, *13*, 601. [[CrossRef](#)]
27. Lin, H.; Muhannad, S.; Derick, B.G.; Kavazanjian, J.R. Mechanical behavior of sands treated by microbially induced carbonate precipitation. *J. Geotech. Geoenviron. Eng.* **2016**, *142*, 015066. [[CrossRef](#)]
28. Cui, M.J.; Zheng, J.J.; Zhang, R.J.; Miao, C.X.; Zhang, J.J. Study of effect of chemical treatment on strength of bio-cemented sand. *Yantu Lixue/Rock Soil Mech.* **2015**, *36*, 392–396.
29. Fu, T.Z.; Saracho, A.C.; Haigh, S.K. Microbially induced carbonate precipitation (MICP) for soil strengthening: A comprehensive review. *Biogeotechnics* **2023**, *1*, 100002. [[CrossRef](#)]
30. Yu, X.P.; Xiao, H.B.; Li, Z.Y.; Qian, J.F.; Luo, S.P.; Su, H.Y. Experimental study on microstructure of unsaturated expansive soil improved by MICP method. *Appl. Sci.* **2022**, *12*, 342. [[CrossRef](#)]
31. Bu, C.M.; Lu, X.Y.; Zhu, D.X.; Liu, L.; Sun, Y.; Wu, Q.T.; Zhang, W.T.; Wei, Q.K. Soil improvement by microbially induced calcite precipitation (MICP): A review about mineralization mechanism, factors, and soil properties. *Arab. J. Geosci.* **2022**, *15*, 863. [[CrossRef](#)]
32. Dagliya, M.; Satyam, N.; Garg, A. Optimization of growth medium for microbially induced calcium carbonate precipitation (MICP) treatment of desert sand. *J. Arid. Land* **2023**, *7*, 797–811. [[CrossRef](#)]
33. Hou, X.K.; Qi, S.W.; Li, T.L.; Guo, S.F.; Wang, Y.; Li, Y.; Zhang, L.X. Microstructure and soil-water retention behavior of compacted and intact silt loess. *Eng. Geol.* **2020**, *277*, 105814. [[CrossRef](#)]
34. GB/T 50123-2019; Ministry of Water Resources of the People's Republic of China, Standard for Geotechnical Test Methods. China Planning Press: Beijing, China, 2019.
35. D2487; Standard Practice for Classification of Soils for Engineering Purposes (Unified Soil Classification System). ASTM (American Society for Testing and Materials): West Conshohocken, PA, USA, 2011.
36. Huang, L.; Gao, Y.F.; Paassen, L.A.V.; He, J.; Wang, L.Y.; Li, C. Microbially induced carbonate precipitation for improving the internal stability of silty sand slopes under seepage conditions. *Acta Geotech.* **2023**, *18*, 2719–2732. [[CrossRef](#)]
37. Xing, W.; Zhou, F.; Zhu, R.; Wang, X.; Chen, T. Performance and mechanism of Zn-contaminated soil through microbe-induced calcium carbonate precipitation. *Buildings* **2023**, *13*, 1974. [[CrossRef](#)]
38. Kang, B.; Zha, F.; Deng, W.; Wang, R.; Sun, X.; Lu, Z. Biocementation of pyrite tailings using microbially induced calcite carbonate precipitation. *Molecules* **2022**, *27*, 3608. [[CrossRef](#)]
39. Li, X.; Wang, Y.; Tang, J.; Li, K. Removal behavior of heavy metals from aqueous solutions via microbially induced carbonate precipitation driven by acclimatized *Sporosarcina pasteurii*. *Appl. Sci.* **2022**, *12*, 9958. [[CrossRef](#)]
40. Ahenkorah, I.; Rahman, M.M.; Karim, M.R.; Beecham, S. Unconfined compressive strength of MICP and EICP treated sands subjected to cycles of wetting-drying, freezing-thawing and elevated temperature: Experimental and EPR modelling. *J. Rock Mech. Geotech. Eng.* **2023**, *5*, 1226–1247. [[CrossRef](#)]
41. Lei, X.G. The types of loess pores in China and their relationship with collapsibility. *Sci. Sin. Ser. B-Chem. Biol. Agric. Med. Earth Sci.* **1988**, *31*, 1398–1410.
42. Chen, P.; Jia, S.G.; Wei, X.Q.; Sun, P.P.; Yi, P.P.; Wei, C.F. Hydraulic path dependence of shear strength for compacted loess. *J. Rock Mech. Geotech. Eng.* **2023**, *7*, 1872–1882. [[CrossRef](#)]
43. Wang, X.M.; Chen, Q.; Chen, X.J.; Zhang, L.M.; Zhou, C.; Wan, L. Experimental study on influence of microbial mineralization on permeability of clay. *Adv. Sci. Technol. Water Resour.* **2024**, *44*, 29–36. (In Chinese)
44. Ouhadi, V.R.; Yong, R.N.; Rafiee, F.; Goodarzi, A.R. Impact of carbonate and heavy metals on micro-structure variations of clayey soils. *Appl. Clay Sci.* **2011**, *52*, 228–234. [[CrossRef](#)]
45. Zha, F.S.; Zhu, F.H.; Kang, B.; Yang, C.B.; Zhang, W.; Zhang, J.W.; Liu, Z.H. Laboratory study of strength, leaching, and electrical resistivity characteristics of heavy-metal contaminated soil. *Environ. Earth Sci.* **2021**, *80*, 184. [[CrossRef](#)]
46. Wang, H.K.; Qian, H.; Gao, Y.Y.; Li, Y.B. Classification and physical characteristics of bound water in loess and its main clay minerals. *Eng. Geol.* **2020**, *265*, 105394. [[CrossRef](#)]
47. Won, C.; Hanlie, H.; Cheng, F.; Fang, Q.; Wang, C.; Zhao, L.; Churchman, J. Clay mineralogy and its palaeoclimatic significance in the Luochuan loess-palaeosols over ~1.3 ma, Shaanxi, northwestern China. *Front. Earth Sci.* **2017**, *12*, 134–147. [[CrossRef](#)]
48. Hong, M.F.; Zhang, L.M.; Tan, Z.X.; Huang, Q.Y. Effect mechanism of biochar's zeta potential on farmland soil's cadmium immobilization. *Environ. Sci. Pollut. Res.* **2019**, *26*, 19738–19748. [[CrossRef](#)]
49. Erdemoglu, M.; Sarikaya, M. Effects of heavy metals and oxalate on the zeta potential of magnetite. *J. Colloid Interface Sci.* **2006**, *300*, 795–804. [[CrossRef](#)]
50. Liao, B.; Li, Y.Y.; Guan, Y.; Liu, Y.H.; Huang, Q.Q.; Ye, C.W.; Liu, G.; Xu, F. Insight into barrier mechanism of fly ash-bentonite blocking wall for lead pollution in groundwater. *J. Hydrol.* **2020**, *590*, 125444. [[CrossRef](#)]

51. Liu, J.D.; Feng, C.; Li, J.S.; Wang, K.K. Soil-water characteristic and microscopic mechanism of arsenic and cadmium composite heavy metal contaminated soil. *Rock Soil Mech.* **2022**, *43*, 2841–2851.
52. Meng, J.; Li, X.A. Effects of carbonate on the structure and properties of loess and the corresponding mechanism: An experimental study of the Malan loess, Xi'an area, China. *Bull. Eng. Geol. Environ.* **2019**, *78*, 4965–4976. [[CrossRef](#)]

Disclaimer/Publisher's Note: The statements, opinions and data contained in all publications are solely those of the individual author(s) and contributor(s) and not of MDPI and/or the editor(s). MDPI and/or the editor(s) disclaim responsibility for any injury to people or property resulting from any ideas, methods, instructions or products referred to in the content.